

## Article

# The Superconducting Dome in Artificial High- $T_c$ Superlattices Tuned at the Fano–Feshbach Resonance by Quantum Design

Gennady Logvenov <sup>1,\*</sup>, Nicolas Bonmassar <sup>1</sup>, Georg Christiani <sup>1</sup>, Gaetano Campi <sup>2,3</sup> , Antonio Valletta <sup>2,4</sup>   
and Antonio Bianconi <sup>2,3,\*</sup> 

- <sup>1</sup> Max Planck Institute for Solid State Research, Heisenbergstraße 1, 70569 Stuttgart, Germany; n.bonmassar@fkf.mpg.de (N.B.); g.cristiani@fkf.mpg.de (G.C.)
- <sup>2</sup> Rome International Center for Materials Science Superstripes RICMASS, Via del Sabelli 119A, 00185 Roma, Italy; gaetano.campi@ic.cnr.it (G.C.); antonio.valletta@artov.imm.cnr.it (A.V.)
- <sup>3</sup> Institute of Crystallography, Italian National Research Council, IC-CNR, Via Salaria Km 29.300, 00015 Roma, Italy
- <sup>4</sup> Institute for Microelectronics and Microsystems, Italian National Research Council IMM-CNR, Via del Fosso del Cavaliere, 100, 00133 Roma, Italy
- \* Correspondence: g.logvenov@fkf.mpg.de (G.L.); antonio.bianconi@ricmass.eu (A.B.)

**Abstract:** While the search for new high-temperature superconductors had been driven by the empirical “trials and errors” method for decades, we now report the synthesis of Artificial High- $T_c$  Superlattices (AHTS) designed by quantum mechanics theory at the nanoscale. This discovery paves the way for engineering a new class of high-temperature superconductors, following the predictions of the Bianconi Perali Valletta (BPV) theory recently implemented in 2022 by Mazziotti et al. including Rashba spin-orbit coupling to create nanoscale AHTS composed of quantum wells. The high- $T_c$  superconducting properties within these superlattices are controlled by a conformational parameter of the superlattice geometry, specifically, the ratio  $L/d$  which represents the thickness of  $\text{La}_2\text{CuO}_4$  layers ( $L$ ) relative to the superlattice period ( $d$ ). Using molecular beam epitaxy, we have successfully grown numerous AHTS samples. These samples consist of initial layers of stoichiometric  $\text{La}_2\text{CuO}_4$  units with a thickness  $L$ , doped by interface space charge, and intercalated with second layers of non-superconducting metallic material,  $\text{La}_{1.55}\text{Sr}_{0.45}\text{CuO}_4$  with thickness denoted as  $W = d - L$ . This configuration forms a quantum superlattice with periodicity  $d$ . The agreement observed between the experimental dependence  $T_c$  (the superconducting transition temperature) versus  $L/d$  ratio and the predictions of the BPV theory for AHTS in the form of the superconducting dome validates the hypothesis that the superconducting dome arises from the Fano–Feshbach or shape resonance in multigap superconductivity driven by quantum nanoscale confinement.

**Keywords:** artificial high  $T_c$  superlattices; Fano-Feshbach resonance; high  $T_c$  superconductivity; quantum confinement; quantum materials design



**Citation:** Logvenov, G.; Bonmassar, N.; Christiani, G.; Campi, G.; Valletta, A.; Bianconi, A. The Superconducting Dome in Artificial High- $T_c$  Superlattices Tuned at the Fano–Feshbach Resonance by Quantum Design. *Condens. Matter* **2023**, *8*, 78. <https://doi.org/10.3390/condmat8030078>

Academic Editor: Carmine Attanasio

Received: 14 August 2023

Revised: 31 August 2023

Accepted: 1 September 2023

Published: 6 September 2023



**Copyright:** © 2023 by the authors. Licensee MDPI, Basel, Switzerland. This article is an open access article distributed under the terms and conditions of the Creative Commons Attribution (CC BY) license (<https://creativecommons.org/licenses/by/4.0/>).

## 1. Introduction

Properties of solids at nanoscale diverge significantly from their bulk counterparts. Interface phenomena encompassing high mobility 2D electron gas (2DEG) [1], superconductivity [2], magnetism [3], and the quantum Hall effect [4] manifest at the interface between  $\text{LaAlO}_3$  and  $\text{SrTiO}_3$ . Quasi-two-dimensional (quasi-2D) high-temperature superconductivity (HTS) emerges at interface between metal/insulator (MI) bilayers. MI bilayers composed of an overdoped  $\text{La}_{1.55}\text{Sr}_{0.45}\text{CuO}_4$  (LSCO) layer, and an undoped  $\text{La}_2\text{CuO}_4$  (LCO) layer show high  $T_c$  interface 2D superconductivity [5], where both individual layers are not superconducting. Detailed investigations of the 2D interface superconductivity [6,7] have focused on understanding superconductivity in two dimensions, giving important information about the control of chemical Sr intermixing across the interface within about one unit cell.

The interface superconductivity was shown to arise from charge transfer at the heterojunction from the metal to the Mott insulator forming the nanoscale interface layer of space charge (holes) within stoichiometric  $\text{La}_2\text{CuO}_4$  [5]. Zn doping reveals that superconductivity is localized around the second  $\text{CuO}_2$  plane from the nominal interface, with the superconducting layer being about two molecular layers (MLs) (two MLs are one unit cell 1.32 nm of the LSCO crystal structure) [8].

Low-energy muon-spin rotation measurements of MI superlattices illustrate antiferromagnetic (AF) ordering in a few-unit-cell-thick  $\text{La}_2\text{CuO}_4$  [9]. The impact of dopant ionic radii on the interface high-temperature superconductivity and the distribution of Ca, Sr, and Ba dopants within 2 nm are explored in diverse MI bilayers ( $\text{La}_{1.55}\text{Ca}_{0.45}\text{CuO}_4/\text{La}_2\text{CuO}_4$ ,  $\text{La}_{1.55}\text{Sr}_{0.45}\text{CuO}_4/\text{La}_2\text{CuO}_4$  and  $\text{La}_{1.55}\text{Ba}_{0.45}\text{CuO}_4/\text{La}_2\text{CuO}_4$ ), employing scanning transmission electron microscopy in combination with electron energy-loss spectroscopy (STEM-EELS) [10]. The superconducting transition temperature ranges from 16 K for Ca-based bilayers to 39 K for Ba-based bilayers. At the LSCO-LCO interface, a  $T_c$  of 40 K is observed across various doping levels in LSCO layers (0.2 to 0.5) in the Sr-rich layer [11]. This observation stimulated several theoretical studies delving into potential scenarios for 2D interface superconductivity [12,13].

The theoretical exploration entails computing charge profiles in LSCO/LCO bilayers [12] grounded on the Poisson equation and doping dependence of the chemical potential obtained by the angle-resolved photoemission spectroscopy in  $\text{La}_{2-x}\text{Sr}_x\text{CuO}_4$  compounds [14]. The microscopic model proposes that 2D interface superconductivity at the natural interface between overdoped non-superconducting  $\text{La}_{2-x}\text{Sr}_x\text{CuO}_4$  and undoped LCO is pinned at the optimal  $T_c$ , irrespective of the carrier concentration in the metallic layer [13].

The notation of “delta-doping” or “modulation” doping originating from semiconductor nanostructures to alter electrical and optical properties [15], has been adopted in cuprate superlattices. Here, the single LaO layer in undoped LCO is replaced with CaO, SrO, BaO, and isovalent DyO layers [16,17]. Layer-dependent superconductivity for divalent dopants (Ca, Sr, and Ba), reaching a maximum  $T_c$  of 35 K with Sr doping, is witnessed.

High-resolution STEM-EELS reveals asymmetric dopant distribution around the Sr-doped layer. The side facing the substrate exhibits distinct Sr-La intermixing (0.9–0.2 nm wide) while the surface-facing side displays diffused intermixing ( $2.3 \pm 0.4$  nm), indicating Sr segregation during the growth. Examination of the O-K edge X-ray absorption spectra discloses the hole concentration profile, signifying a superconducting space-charge accumulation layer of about 2.6 nm on the side of the chemically undoped  $\text{La}_2\text{CuO}_4$  layer, as expected in a p-n junction [16–18]. The interplay between high- $T_c$  superconductivity and antiferromagnetic order in these Sr-doped superlattices has been investigated via low-energy muon spin rotation [19].

The 2DEG at the  $\text{SrTiO}_3$  interface shows a superconducting dome of  $T_c$  versus charge density, which has been assigned [20] to a Fano–Feshbach resonance or shape resonance between superconducting gaps near a Lifshitz transition for electronic topological transformation of “opening a neck in the appearing Fermi surface” using the Bianconi Perali Valletta (BPV) theory for superlattices of quantum wires [21–23], extended to superlattices of quantum wells [24] as a case of multigap high- $T_c$  superconductivity near the BCS-BEC crossover [25–28] where the apex of the superconductivity dome is steered by quantum size effects, pair exchange interaction between gaps and, more recently, it has been shown to be amplified by the Rashba spin-orbit coupling (SOC) [29,30]. This coupling stems from the internal electric field in nanoscale heterojunctions formed at the interfaces between different materials, tied to the adjoining space charge layer. It has been shown that the multigap superconductivity [20,28] at the interface is determined by the formation of subbands due to quantum size effects determined by the nanoscale thickness of the 2DEG interface.

Here we provide novel artificial high- $T_c$  superlattices (AHTS) using the advanced BPV theory [30] to design superlattices of quantum wells tuned at the Fano-Feshbach resonance [31] formed by using two different non-superconducting cuprate compounds;

therefore, they can be considered as superconductors with artificially designed nanoscale phase separation. Thus, this work provides evidence that the nanoscale chemical phase separation observed in different types of multigap high- $T_c$  superconductors, including  $\text{MgB}_2$  doped by Sc or Al [32] or cuprates doped by oxygen interstitials [33,34] and iron based superconductors [35], can tune superconducting properties via the Fano–Feshbach resonances. Following our presented results many different AHTS made of heterogeneous systems with artificial multiband interface charge layers can be grown by using modern synthesis techniques [36]. By tuning the electronic properties of these layers and quantum size effects, one can control the Fano–Feshbach resonances at nanoscale [21–29] and obtain high temperature superconductivity in AHTS. This could open a new direction (era) of search of superconducting quantum materials with  $T_c$  on demand driven by quantum mechanics theory.

## 2. Results and Discussion

The central objective of this study was to experimentally validate the quantitative predictions of the superconducting dome in AHTS [29,30]. These predictions are based on the deliberate design of nanoscale LSCO/LCO superlattices, wherein the superconducting layers (S) consist of a 2D electron gas (2DEG) formed by the interface space charge. The 2DEG has a thickness denoted as  $L$  and is confined in LCO layers, while being sandwiched by metallic LSCO layers in the LSCO/LCO superlattices. The overall superlattice structure has a periodicity represented as  $d$  in Figure 1. The primary approach taken was to compute the high- $T_c$  superconducting dome utilizing the BPV theory for a superlattice of quantum wells, which mimics the structure of the LSCO/LCO superlattice.

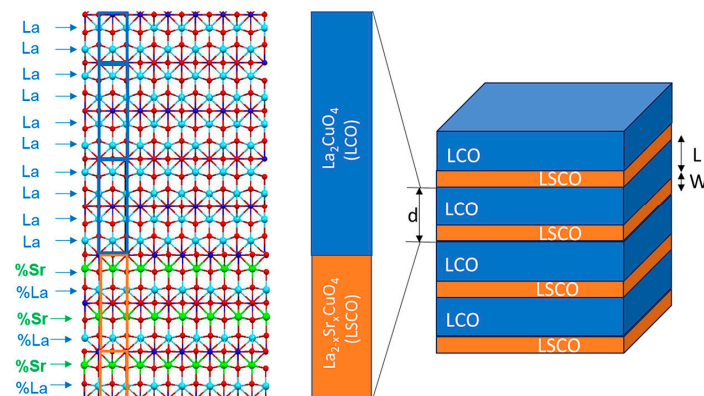


**Figure 1.** Pictorial view of an AHTS superconductor showing a practical realization of the nanoscale AHTS of the type called three dimensional (3D) superlattice of quantum wells made of five ML ( $L = 3.3$  nm) of undoped LCO, electronically doped by the interface space charge, which are intercalated by normal metal units made of three ML ( $W = 1.98$  nm) of LSCO forming a superlattice with a period of  $d = L + W = 5.28$  nm and with conformational parameter  $L/d = 5/8 = 0.625$  giving the optimum critical temperature appearing in the range  $0.6 < L/d < 0.7$ .

The theoretical critical temperature,  $T_c$ , has been plotted as a function of the  $L/d$  conformational parameter, which characterizes the geometry of the superlattice, thereby yielding the superconducting dome  $T_c(L/d)$ . In parallel, the experimental critical temperature dome,  $T_c(L/d)$ , was determined through measurements on LSCO/LCO superlattices fabricated using molecular beam epitaxy (MBE). Our focus has been directed to superlattices with maximum periods,  $d$ , ranging up  $\sim 5$  nm. Figure 1 provides an illustrative depiction of a typical LSCO/LCO superlattice with a period of  $d = 5.28$  nm. In this configuration, the LCO layer has a thickness of five molecular layers (ML), denoted as  $L = 3.3$  nm, and the LSCO layer has a thickness of three ML, indicated as  $W = 1.98$  nm.

Our experimental approach was based on the idea of manipulation of the 2DEG interface space charge layer, which spread within a 2.6 nm thickness in the LCO layer,

from the LSCO/LCO interface. The quantum confinement of this layer between two LSCO potential barriers,  $V$ , in the superlattice creates two artificial subbands due to quantum size effects and modulates either their energy splitting or the potential barrier transparency by tuning thickness ratio,  $L/d$ .

### 2.1. Quantum Design of AHTS

The quantum material design of AHTS shown in Figure 1 has been carried out by first-principle quantum mechanics numerical calculations of electronic and superconducting properties shown in Figure 2 using the BPV theory [21–23,29,30].

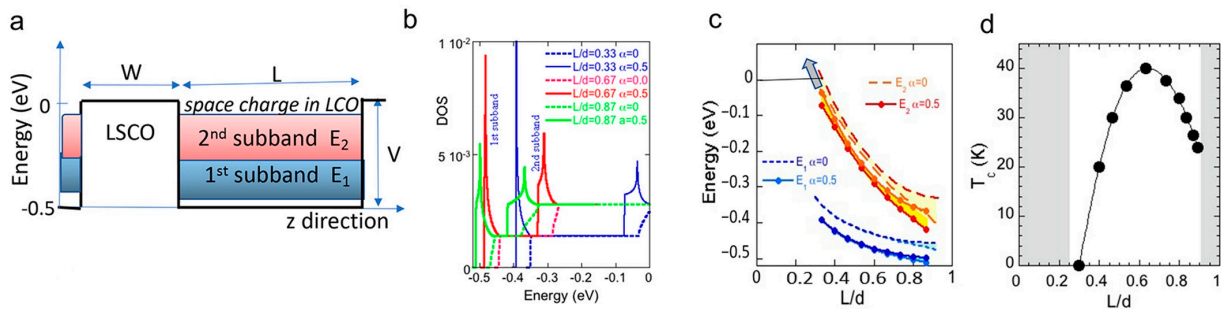


**Figure 2.** (a) The periodic electronic band structure in the LSCO/LCO artificial superlattice. The potential barrier of 500 meV is developed in LSCO layers, while in the superconducting LCO space charge layer for the ratio  $L/d$  between 0.25 and 0.9 the quantum confinement in the potential well  $L$  gives two electronic subbands with band edges at  $E_1$  and  $E_2$ . (b) The density of states (DOS) of the LCO quantum wells in LCO/LSCO superlattices with different conformational parameters  $L/d$  for  $L/d = 0.67$  in red corresponds to the case with maximum  $T_c$ , for  $L/d = 0.87$  in green and for  $L/d = 0.33$  in blue, correspond to cases with reduced  $T_c$ . The DOS calculations with same  $L/d$  parameter with SOC,  $\alpha = 0.5$  are shown with solid lines and with no SOC,  $\alpha = 0$  is shown as dashed line with the same color. (c) Energy values of the energies  $E_1$  and  $E_2$  of the Lifshitz transition for appearing of a new Fermi surface and for opening a neck in the Fermi surface in the lower  $E_1$  and upper  $E_2$  electronic subbands without SOC,  $\alpha = 0$  (dashed lines), and with SOC,  $\alpha = 0.5$  (solid lines). (d) The superconductivity dome of the critical temperature  $T_c$  predicted by the BPV theory at a Fano–Feshbach resonance for the superlattice of quantum wells as a function of  $L/d$  in the range of  $0.25 < L/d < 0.9$ .

In multigap superconductivity [24–29] the configuration interaction between gaps in flat and steep bands or between different Fermi surfaces via the Fano–Feshbach resonance could tune superconducting properties. The  $T_c$  superconducting dome as a function of doping or pressure in unconventional high- $T_c$  superconductors is considered the hallmark of a mysterious strange metal phase giving high temperature superconductivity.

The quantum numerical calculations of the Fano–Feshbach resonance [29,30], including SOC, have been carried out for a superlattice of quantum wells of period  $d = 3$  nm and variable potential well thickness  $0.75 < L < 2.7$  nm of the superconductor layer, with a conformational ratio of  $0.25 < L/d < 0.9$ .

The superconducting layer has been assumed to be confined within the potential barrier of 500 meV, at the interface between LCO and LSCO oxide layers [14,37], as in a recent work [30]. We studied AHTS made of the superlattice of quantum wells with  $d = 3$  nm for variable  $0.24 < L/d < 0.9$  [29,30], giving the two subbands generating the two gap superconductivity, which shows a superconducting dome of the critical temperature  $T_c$  as a function of both charge density and pairing strength  $g$  with maximum  $T_c = 40$  K. We used a weak  $g = 0.3$  pairing strength in the small Fermi surface in the second upper subband, and weak pair exchange non-diagonal terms in the coupling tensor, which have been shown to give 40 K superconductivity [29,30].

The results of our calculations of the critical temperature as a function of  $L/d$  ratio with a fixed potential barrier of quantum wells 500 meV and the intraband pairing coupling  $g = 0.3$  including SOC constant  $\alpha = 0.5$  are shown in panel (d) of Figure 2 [30].

The superconducting dome has been assigned to a variety of possible quantum critical points object of controversy between different authors.

In our BPV theory, the  $T_c$  dome, is determined by the Fano–Feshbach resonance controlled by the superlattice geometry, charge density, pairing strength and Rashba spinorbit coupling [29,30].

According to these calculations (Figure 2), the two-gap superconductivity regime is present only in the range of  $0.25 < L/d < 0.9$  in nanoscale AHTS. For  $L/d < 0.25$ , the second subband is pushed up in the continuum because of a narrow  $L$  width, and the finite potential barrier  $V$  of the superlattice entering in a single gap regime. On the other side of the dome, for  $L/d > 0.9$ , the width of the metallic LSCO layer  $W$  becomes very thin and transparent; therefore, the two wide subbands merge in a single band.

## 2.2. MBE Synthesis of Artificial High- $T_c$ Superlattices

AHTS based on normal metal LSCO and superconducting space charge layer formed in LCO thin layers have been synthesized via an ozone-assisted MBE method (DCA Instruments Oy) on LaSrAlO<sub>4</sub> (001) substrates (compressive strain for La<sub>2</sub>CuO<sub>4</sub> on LaSrAlO<sub>4</sub> is +1.4%).

The superlattice growth was controlled by the in situ reflection high-energy electron diffraction (RHEED). This method is characterized by the sequence of deposition of single atomic layers and minimal kinetic energy of impinging atoms (about 0.1 eV). The substrate temperature  $T_s$  according to radiation pyrometer reading was 650 °C, and the chamber pressure  $p \approx 1.5 \times 10^{-5}$  Torr of mixed ozone, atomic and molecular oxygen.

After finishing, the growth samples were cooled down to  $T_s = 200$  °C. The delivery of ozone was stopped at this temperature and, thereafter, samples were cooled down in vacuum to remove the interstitial oxygen in La<sub>2</sub>CuO<sub>4</sub> layers and to make these layers undoped. The high-quality crystal superlattice structure of the AHTS was confirmed by X-ray diffraction and reflectivity measured by using Bruker D8 Cu <sub>$\alpha$ ,1</sub> = 1.5406 Å shown in Figure 3.

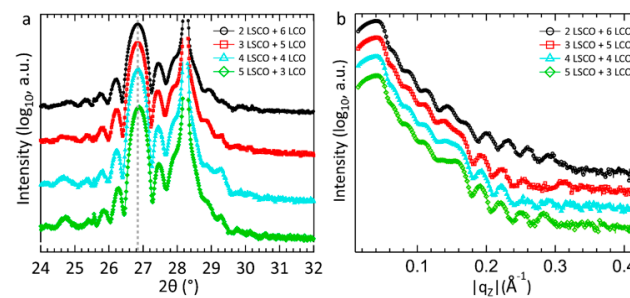


**Figure 3.** (a) X-ray diffraction (XRD), (b) X-ray Reflectivity (XRR) of AHTS. Black circles, red squares, turquoise triangles and green deltsoids correspond to XRD and XRR for different superlattices with a constant period  $d = 8$  ML, and different  $L/d$  ratios. AHTS are classified as  $m$ LSCO +  $n$ LCO, where  $m$  and  $n$  are integer numbers of ML of LSCO and LCO, correspondingly.

## 2.3. The Superconducting Dome of AHTS

Temperature dependence of resistance were performed in a four-point van der Pauw configuration with alternative DC current  $\pm 10$   $\mu$ A in a temperature range from room temperature to 4.2 K (liquid helium). Simultaneously, the mutual inductance of real and imaginary part of AC magnetic susceptibility was measured in a two-coil configuration with alternative current in driving coil of 50  $\mu$ A and frequency 1000 Hz. Both temperature dependent resistance and mutual inductance were measured simultaneously by using

a motorized custom-made dipstick in a transport helium dewar with temperature rate  $<0.1$  K/s.

Figure 4a depicts the normalized sheet resistance as a function of temperature of different AHTS consisting of electronic doped LCO quantum wells between metallic LSCO layers with fixed period  $d = 5.28$  nm and various  $L/d$  ratios. AHTS exhibiting a maximum  $T_c$  with  $L/d = 0.625$ – $0.75$  ratios show linear temperature dependences, as shown by the dashed line in Figure 4a. The linear temperature dependence of resistance ( $T$ -linear regime) indicates that the scattering rate hits the Planckian limit, [38,39] given by  $\hbar/\tau = K_B T$  that is expected to occur at the unconventional extended van Hove singularity for a Lifshitz transition of the opening a neck type, while it was considered the hallmark of the strange metal phase in HTS cuprates. In our AHTS, the  $T$ -linear regime appears where the critical temperature is at its maximum value. Figure 4b shows the experimental critical temperature  $T_c$  versus  $L/d$  data, giving a superconducting dome for a fixed superlattice period  $d = 5.28$  nm that is quantitatively agreeing with our theoretical curve (dashed line) presented in Figure 2c. The universal superconducting dome of  $T_c$  versus  $L/d$  ratios for all LSCO/LCO superlattices studied in this work with slightly different periods in the range of  $1.98 < d < 5.28$  nm is presented in Figure 4c. These results provide compelling evidence for the high- $T_c$  quantum amplification mechanism driven by a Fano–Feshbach or shape resonance in multi-gap superconductors [31] with the key role of quantum geometry control of the superconducting transition temperatures in AHTS.

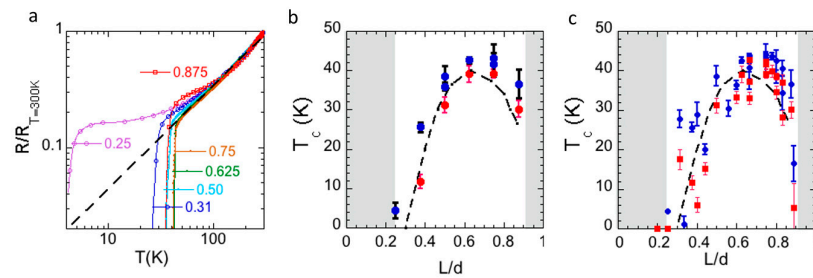


**Figure 4.** (a) The normalized sheet resistance as a function of temperature of LSCO/LCO superlattices with a constant period  $d = 5.28$  nm and different  $L/d$ . ( $R_{300}$  is the resistance measured at 300 K).  $L/d = 0.25$  (violet color), corresponds to the overdoped regime and  $L/d = 0.875$  (red color) corresponds to the underdoped regime of the HTS phase diagram of cuprates, both with reduced  $T_c$ . The maximum  $T_c \approx 43$  K observed at  $L/d = 0.625$ – $0.75$  corresponds to a critical temperature in the optimum doped LSCO. (b) The critical temperature determined as maximum of a derivative of the sheet resistance (blue dots) and maximum of imaginary part of the mutual inductance (red dots). (c)  $T_c$  versus  $L/d$  for all LSCO/LCO superlattices with a different period in the range from 1.98 nm to 5.28 nm. The dashed curve in panels (b,c) are the theory predictions using the BPV theory including a SOC as shown in Figure 2.

### 3. Conclusions

In conclusion, this work offers compelling experimental validation for the quantum material design and predictions pertaining to nanoscale AHTS based on the BPV theory. These predictions, rooted in calculations of the resonant quantum tunneling within superlattices of quantum wells in LCO layers hosting the interface space charge, have been realized through a growth process involving alternating layers of metallic LSCO and undoped LCO layers. Many AHTS with varying periods within the range of  $1.98 < d < 5.28$  nm have been synthesized using ozone-assisted MBE.

The study reveals tunable high- $T_c$  superconductivity with a universal dome-like dependence of  $T_c$  on the superlattice period and layer thickness. Additionally, the unconventional linear temperature dependence of the normal state resistance is observed for superlattices with the highest  $T_c$ , indicating the attainment of the Planckian scattering rate limit.

The engineered AHTS, composed of different non-superconducting cuprate compounds, can be regarded as superconductors exhibiting artificial nanoscale phase separation. Therefore they shed light on the role of arrested nanoscale chemical (or extrinsic) phase separation revealed in natural high  $T_c$  superconductors by local structural probes [32–35] where only short range superstructure is observed but correlated disorder allows 3D percolation of nanoscale puddles tuned at the Fano-Feshbach resonance [40]. Finally this work demonstrates the potential of manipulating nanoscale chemical phase separation to tune superconducting properties through the Fano–Feshbach resonance between superconducting gaps, suggesting a new avenue for the exploration of superconducting quantum materials with controllable  $T_c$ , guided by quantum mechanics theory.

**Author Contributions:** Conceptualization, A.B. and G.L.; methodology, G.L. and A.B.; software, A.V., G.C. (Gaetano Campi) and A.B.; validation, G.L. and A.B.; formal analysis, G.L., G.C. (Gaetano Campi), A.B. and N.B.; investigation, G.L., N.B., G.C. (Georg Christiani), G.C. (Gaetano Campi), A.V. and A.B.; sample synthesis, G.L., N.B. and G.C. (Georg Christiani); data curation, G.L., N.B., G.C. (Georg Christiani), G.C. (Gaetano Campi) and A.B.; writing—original draft preparation A.B., G.L., N.B. and G.C. (Gaetano Campi); writing—review and editing, G.L., A.B., N.B., G.C. (Georg Christiani) and G.C. (Gaetano Campi). All authors have read and agreed to the published version of the manuscript.

**Funding:** This research received funding from Superstripes onlus.

**Institutional Review Board Statement:** Not applicable.

**Informed Consent Statement:** Not applicable.

**Data Availability Statement:** The data that support the findings of this study are available from the corresponding author (A.B.) upon reasonable request.

**Acknowledgments:** We thank Andrea Perali for useful discussions.

**Conflicts of Interest:** The authors declare no conflict of interest. The funders had no role in the design of the study; in the collection, analyses, or interpretation of data; in the writing of the manuscript; or in the decision to publish the results.

## References

1. Ohtomo, A.; Hwang, H.Y. A high mobility electron gas at the  $\text{LaAlO}_3/\text{SrTiO}_3$  heterointerface. *Nature* **2004**, *427*, 423–426. [[CrossRef](#)] [[PubMed](#)]
2. Reyren, N.; Thiel, S.; Caviglia, A.D.; Kourkoutis, L.F.; Hammerl, G.; Richter, C.; Schneider, C.W.; Kopp, T.; Ruetschi, A.S.; Jaccard, D.; et al. Superconducting interfaces between insulating oxides. *Science* **2007**, *317*, 1196–1199. [[CrossRef](#)] [[PubMed](#)]
3. Brinkman, A.; Huijben, M.; Van Zalk, M.; Huijben, J.; Zeitler, U.; Maan, J.C.; van der Wiel, W.G.; Rijnders, G.J.; Blank, D.H.; Hilgenkamp, H. Magnetic effects at the interface between non-magnetic oxides. *Nat. Mater.* **2007**, *6*, 493–496. [[CrossRef](#)]
4. Tsukazaki, A.; Ohtomo, A.; Kita, T.; Ohno, Y.; Ohno, H.; Kawasaki, M. Quantum Hall Effect in Polar Oxide Heterostructures. *Science* **2007**, *315*, 1388–1391. [[CrossRef](#)] [[PubMed](#)]
5. Gozar, A.; Logvenov, G.; Kourkoutis, L.F.; Bollinger, A.T.; Giannuzzi, L.A.; Muller, D.A.; Bozovic, I. High temperature interface superconductivity between metallic and insulating copper oxides. *Nature* **2008**, *455*, 782–785. [[CrossRef](#)] [[PubMed](#)]
6. Pereiro, J.; Bollinger, A.T.; Logvenov, G.; Gozar, A.; Panagopoulos, C.; Božović, I. Insights from the study of high temperature interface superconductivity. *Phil. Trans. R. Soc.* **2012**, *370*, 4890–4903. [[CrossRef](#)]
7. Smadici, S.J.; Lee, J.C.; Wang, S.; Abbamonte, P.; Logvenov, G.; Gozar, A.; Cavellin, C.D.; Bozovic, I. Superconducting transition at 38 K in insulating-overdoped  $\text{La}_2\text{CuO}_4\text{-La}_{1.64}\text{Sr}_{0.36}\text{CuO}_4$  superlattices: Evidence for electronic redistribution from resonance soft X-ray scattering. *Phys. Rev Lett.* **2009**, *102*, 107004. [[CrossRef](#)]
8. Logvenov, G.; Gozar, A.; Bozovic, I. High-temperature superconductivity in a single copper-oxygen plane. *Science* **2009**, *326*, 699–7023. [[CrossRef](#)]
9. Suter, A. Two-dimensional magnetic and superconducting phases in metal-insulator  $\text{La}_{2-x}\text{Sr}_x\text{CuO}_4$  superlattices measured by muon-spin rotation. *Phys. Rev. Lett.* **2011**, *106*, 237003. [[CrossRef](#)]
10. Suyolcu, Y.E.; Wang, Y.; Baiutti, F.; Al-Temimy, A.; Gregori, G.; Cristiani, G.; Sigle, W.; Maier, J.; van Aken, P.A.; Logvenov, G. Dopant size effects on novel functionalities: High-temperature interface superconductivity. *Sci. Rep.* **2017**, *7*, 453. [[CrossRef](#)]
11. Wu, J.; Pelleg, O.; Logvenov, G.; Bollinger, A.T.; Sun, Y.J.; Boebinger, G.S.; Vanević, M.; Radović, Z.; Božović, I. Anomalous independence of interface superconductivity from carrier density. *Nat. Mater.* **2013**, *12*, 877–881. [[CrossRef](#)] [[PubMed](#)]
12. Radovic, Z.; Vanevic, M.; Bollinger, A.T.; Bozovic, I. Interface superconductivity in cuprate defies Fermi-liquid description. *J. Supercond. Nov. Magn.* **2017**, *30*, 725–729. [[CrossRef](#)]

13. Misawa, T.; Nomura, Y.; Biermann, S.; Imada, M. Self-optimized superconductivity attainable by interlayer phase separation at cuprate interfaces. *Sci. Adv.* **2016**, *2*, e1600664. [[CrossRef](#)]
14. Ino, A.; Mizokawa, T.; Fujimori, A.; Tamasaku, K.; Eisaki, H.; Uchida, S.; Kimura, T.; Sasagawa, T.; Kishio, K. Chemical potential shift in overdoped and underdoped  $\text{La}_{2-x}\text{Sr}_x\text{CuO}_4$ . *Phys. Rev. Lett.* **1997**, *79*, 2101. [[CrossRef](#)]
15. Harris, J.J. Review Delta-doping of semiconductors. *J. Mater. Sci. Mater. Electron.* **1993**, *4*, 93–105. [[CrossRef](#)]
16. Baiutti, F.; Logvenov, G.; Gregori, G.; Cristiani, G.; Wang, Y.; Sigle, W.; van Aken, P.A.; Maier, J. High-temperature superconductivity in space-charge regions of lanthanum cuprate induced by two-dimensional doping. *Nat. Commun.* **2015**, *6*, 8586–8593. [[CrossRef](#)]
17. Baiutti, F.; Gregori, G.; Wang, Y.; Suyolcu, Y.E.; Cristiani, G.; van Aken, P.A.; Maier, J.; Logvenov, G. Cationic redistribution at epitaxial interfaces in superconducting two-dimensional doped lanthanum cuprate films. *ACS Appl. Mater. Interfaces* **2016**, *8*, 27368–27375. [[CrossRef](#)]
18. Suyolcu, Y.E.; Cristiani, G.; van Aken, P.A.; Logvenov, G. Design of complex oxide interfaces by oxide molecular beam epitaxy. *J. Supercond. Nov. Magn.* **2020**, *33*, 107–120. [[CrossRef](#)]
19. Suter, A.; Logvenov, G.; Boris, A.V.; Baiutti, F.; Wrobel, F.; Howald, L.; Stilp, E.; Salman, Z.; Prokscha, T.; Keimer, B. Superconductivity drives magnetism in  $\delta$ -doped  $\text{La}_2\text{CuO}_4$ . *Phys. Rev. B* **2018**, *97*, 134522. [[CrossRef](#)]
20. Bianconi, A.; Innocenti, D.; Valletta, A.; Perali, A. Shape Resonances in superconducting gaps in a 2DEG at oxide-oxide interface. *J. Phys. Conf. Ser.* **2014**, *529*, 012007. [[CrossRef](#)]
21. Bianconi, A.; Valletta, A.; Perali, A.; Saini, N.L. Superconductivity of a striped phase at the atomic limit. *Phys. C Supercond.* **1998**, *296*, 269–280. [[CrossRef](#)]
22. Perali, A.; Bianconi, A.; Lanzara, A.; Saini, N.L. The gap amplification at a shape resonance in a superlattice of quantum stripes: A mechanism for high  $T_c$ . *Solid State Commun.* **1996**, *100*, 181–186. [[CrossRef](#)]
23. Valletta, A.; Bianconi, A.; Perali, A.; Saini, N.L. Electronic and superconducting properties of a superlattice of quantum stripes at the atomic limit. *Z. Für Phys. B Condens. Matter* **1997**, *104*, 707–771. [[CrossRef](#)]
24. Innocenti, D.; Poccia, N.; Ricci, A.; Valletta, A.; Caprara, S.; Perali, A.; Bianconi, A. Resonant and crossover phenomena in a multiband superconductor: Tuning the chemical potential near a band edge. *Phys. Rev. B* **2010**, *82*, 184528. [[CrossRef](#)]
25. Ochi, K.; Tajima, H.; Iida, K.; Aoki, H. Resonant pair-exchange scattering and BCS-BEC crossover in a system composed of dispersive and heavy incipient bands: A Feshbach analogy. *Phys. Rev. Res.* **2022**, *4*, 013032.e26. [[CrossRef](#)]
26. Cariglia, M.; Vargas-Paredes, A.; Doria, M.M.; Bianconi, A.; Milošević, M.V.; Perali, A. Shape-resonant superconductivity in nanofilms: From weak to strong coupling. *J. Supercond. Nov. Magn.* **2016**, *29*, 3081–3086. [[CrossRef](#)]
27. Salasnich, L.; Shanenko, A.A.; Vagov, A.; Aguiar, J.A.; Perali, A. Screening of pair fluctuations in superconductors with coupled shallow and deep bands: A route to higher-temperature superconductivity. *Phys. Rev. B* **2019**, *100*, 064510. [[CrossRef](#)]
28. Valentini, D.; Gariglio, S.; Fête, A.; Triscone, J.M.; Berthod, C.; Van Der Marel, D. Modulation of the superconducting critical temperature due to quantum confinement at the  $\text{LaAlO}_3/\text{SrTiO}_3$  interface. *Phys. Rev. B* **2017**, *96*, 094518. [[CrossRef](#)]
29. Mazziotti, M.V.; Valletta, A.; Raimondi, R.; Bianconi, A. Multigap superconductivity at an unconventional Lifshitz transition in a three-dimensional Rashba heterostructure at the atomic limit. *Phys. Rev. B* **2021**, *103*, 024523. [[CrossRef](#)]
30. Mazziotti, M.V.; Bianconi, A.; Raimondi, R.; Campi, G.; Valletta, A. Spin-orbit coupling controlling the superconducting dome of artificial superlattices of quantum wells. *J. Appl. Phys.* **2022**, *132*, 193908. [[CrossRef](#)]
31. Bianconi, A. High  $T_c$  Superconductors Made by Metal Heterostructures at the Atomic Limit. European Patent N. EP0733271; (priority date 7 December 1993), Available online: <https://patents.google.com/patent/EP0733271A1> (accessed on 25 September 1996).
32. Agrestini, S.; Metallo, C.; Filippi, M.; Simonelli, L.; Campi, G.; Sanipoli, C.; Liarokapis, E.; De Negri, S.; Giovannini, M.; Saccone, A.; et al. Substitution of Sc for Mg in  $\text{MgB}_2$ : Effects on transition temperature and Kohn anomaly. *Phys. Rev. B* **2004**, *70*, 134514. [[CrossRef](#)]
33. Fratini, M.; Poccia, N.; Ricci, A.; Campi, G.; Burghammer, M.; Aeppli, G.; Bianconi, A. Scale-free structural organization of oxygen interstitials in  $\text{La}_2\text{CuO}_{4+y}$ . *Nature* **2010**, *466*, 841–844. [[CrossRef](#)] [[PubMed](#)]
34. Campi, G.; Bianconi, A.; Poccia, N.; Bianconi, G.; Barba, L.; Arrighetti, G.; Innocenti, D.; Karpinski, J.; Zhigadlo, N.D.; Kazakov, S.M.; et al. Inhomogeneity of charge-density-wave order and quenched disorder in a high- $T_c$  superconductor. *Nature* **2015**, *525*, 359–362. [[CrossRef](#)]
35. Ricci, A.; Poccia, N.; Campi, G.; Joseph, B.; Arrighetti, G.; Barba, L.; Reynolds, M.; Burghammer, M.; Takeya, H.; Mizuguchi, Y.; et al. Nanoscale phase separation in the iron chalcogenide superconductor  $\text{K}_{0.8}\text{Fe}_{1.6}\text{Se}_2$  as seen via scanning nanofocused X-ray diffraction. *Phys. Rev. B* **2011**, *84*, 060511. [[CrossRef](#)]
36. Thapa, S.; Paudel, R.; Blanchet, M.D.; Gemperline, P.T.; Comes, R.B. Probing surfaces and interfaces in complex oxide films via in situ X-ray photoelectron spectroscopy. *J. Mater. Res.* **2021**, *36*, 26–51. [[CrossRef](#)]
37. Yunoki, S.; Moreo, A.; Dagotto, E.; Okamoto, S.; Kancharla, S.S.; Fujimori, A. Electron doping of cuprates via interfaces with manganites. *Phys. Rev. B* **2007**, *76*, 064532. [[CrossRef](#)]
38. Zaanen, J. Planckian dissipation, minimal viscosity and the transport in cuprate strange metals. *SciPost Phys.* **2019**, *6*, 061. [[CrossRef](#)]

39. Yuan, J.; Chen, Q.; Jiang, K.; Feng, Z.; Lin, Z.; Yu, H.; He, G.; Zhang, J.; Jiang, X.; Zhang, X.; et al. Scaling of the strange-metal scattering in unconventional superconductors. *Nature* **2022**, *602*, 431–436. [[CrossRef](#)]
40. Campi, G.; Mazziotti, M.V.; Jarlborg, T.; Bianconi, A. Scale-free distribution of oxygen interstitial wires in optimum-doped  $\text{HgBa}_2\text{CuO}_{4+y}$ . *Condens. Matter* **2022**, *7*, 56. [[CrossRef](#)]

**Disclaimer/Publisher’s Note:** The statements, opinions and data contained in all publications are solely those of the individual author(s) and contributor(s) and not of MDPI and/or the editor(s). MDPI and/or the editor(s) disclaim responsibility for any injury to people or property resulting from any ideas, methods, instructions or products referred to in the content.